Ar Solvation Shells in K+−HFBz: From Cluster Rearrangement to Solvation Dynamics

ARTICLE *in* THE JOURNAL OF PHYSICAL CHEMISTRY A · SEPTEMBER 2011

Impact Factor: 2.69 · DOI: 10.1021/jp206601m · Source: PubMed

3 AUTHORS, INCLUDING:

Margarita Albertí Wirsing
University of Barcelona
91 PUBLICATIONS **939** CITATIONS
SEE PROFILE

Noelia Faginas Lago
Università degli Studi di Perugia
48 PUBLICATIONS **250** CITATIONS
SEE PROFILE

THE JOURNAL OF PHYSICAL CHEMISTRY A

ARTICLE

pubs.acs.org/JPCA

Ar Solvation Shells in K^+—HFBz: From Cluster Rearrangement to Solvation Dynamics

M. Albertí,*[,†] N. Faginas Lago,[‡] and F. Pirani[‡]

[†]IQTCUB, Departament de Química Física, Universitat de Barcelona, Barcelona, Spain

[‡]Dipartimento di Chimica, Università di Perugia, Perugia, Italy

ABSTRACT: The effect of some leading intermolecular interaction components on specific features of weakly bound clusters involving an aromatic molecule, a closed shell ion, and Ar atoms is analyzed by performing molecular dynamics simulations on potential energy surfaces properly formulated in a consistent way. In particular, our investigation focuses on the three-dimensional Ar distributions around the K^+—hexafluorobenzene (K^+—HFBz) dimer, in K^+-HFBz-Ar_n aggregates ($n \leq 15$), and on the gradual evolution from cluster rearrangement to solvation dynamics when ensembles of 50, 100, 200, and 500 Ar atoms are taken into account. Results indicate that the Ar atoms compete to be placed in such a way to favor an attractive interaction with both K^+ and HFBz, occupying positions above and below the aromatic plane but close to the cation. When these positions are already occupied, the Ar atoms tend to be placed behind the cation, at larger distances from the center of mass of HFBz. Accordingly, three different groups of Ar atoms are observed when increasing n, with two of them surrounding K^+, thus, disrupting the K^+—HFBz equilibrium geometry and favoring the dissociation of the solvated cation when the temperature increases. The selective role of the leading intermolecular interaction components directly depending on the ion size repulsion is discussed in detail by analyzing similarities and differences on the behavior of the Ar-solvated K^+—HFBz and Cl^-—Bz aggregates.

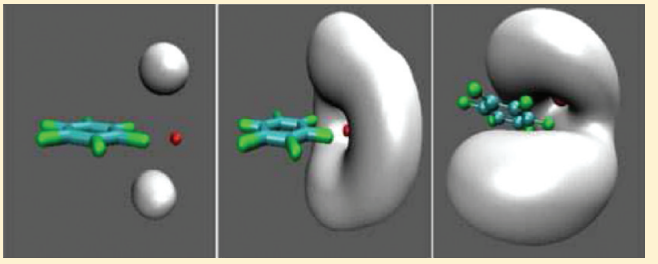

1. INTRODUCTION

Chemical dynamics is a branch of physical chemistry that seeks to explain time-dependent phenomena, such as energy transfer and chemical reactivity, in terms of the detailed motion of the nuclei and electrons constituting the system. From an experimental point of view, the crossed molecular beams technique allows the investigation of several processes such as capture and electronic excitation[1] and chemical reactions (see for instance[2]) in great detail. On the other hand, the reactivity of the systems can also be investigated from theoretical methodologies (classical and quantum approaches), for example cross sections, rate coefficients, and energy distributions, which can be calculated by means of quasiclassical trajectories (see, for instance, refs 3−6) and quantum and semiclassical methods (see, for instance, ref 7) whose results can be tested from available experimental data. However, these theoretical methodologies can only be applied to the study of small systems. Accordingly, more complex systems and processes involving several chemical dynamics aspects should be investigated by using molecular dynamics (MD) methodologies. However, the application of such methodologies often requires the use of intermolecular potential energy surfaces formulated as a combination of semiempirical and empirical functions having continuous derivatives and able to describe in a consistent way the full configuration space, including associative, dissociative, and isomerization channels.

MD is indeed an important tool for characterizing structure, dynamics, and thermodynamics of complex processes as those occurring in biological systems, for instance, solvation phenomena, whose extent depends on the characteristics of both solvated species (solute) and solvent. As a matter of fact, the solvation leads to a specific region around the solute, which is characterized by the particular structure of the solvent (around molecules) in respect of pure solvent. In particular, when ions are involved and solvent is liquid water, the solvation region close the ions is strongly influenced by electrostatic interactions, causing a strong directionality of the intermolecular bonds in the ligand network. The inert gas atoms, with their formally filled valence shell, can be considered the simplest but suitable prototypes for modeling solvation processes, without any electrostatic contamination.[8] In spite of the fact that induction and electrostatic forces can play an important role in solvation processes (not present in Ar—Ar interactions), Ar atoms can be taken as surrogates of water molecules, mainly because of their similar polarizability. However, it must be taken into account that orientational effects of the solvent, due to the electrostatic interactions, are absent when using Ar atoms. The microsolvation of ions in argon has been widely investigated by means of both experimental techniques[9−12] and theoretical methods.[13−18] A recent study of the solvated Na^+-Cl^--Bz aggregate and of the involved fragments, Na^+—Bz and Cl^-—Bz, showed that the solvation is strongly affected by the

Received: July 12, 2011
Revised: August 28, 2011
Published: September 01, 2011

most stable structures of the unsolvated systems.[19] It was observed that the most stable on plane bifurcated structure of Cl^-—Bz originates less compact solvation shells than Na^+—Bz, the latter having the equilibrium configuration in which the cation is placed along the C_6 axis of Bz. The different equilibrium geometry of the halide-Bz and alkali cation-Bz can be interpreted from the capability as electron donor of the Bz π electronic cloud. As a matter of fact, hexafluorobenzene (HFBz), with a quadrupole moment of 9.50 B,[20] comparable in magnitude with that of Bz equal to −8.45 B[21,22] but opposite in sign, forms equilibrium on plane bifurcated structures when interacting with alkali cations. The different sign of the quadrupole moments suggests that for HFBz the positive regions of Bz, representative of a defect in the electron charge distribution, become negative and the negative positive.[22] Due to the high values of the Bz and HFBz quadrupole moments, it was believed that the electrostatic interaction was the major source of the attraction in cation−π interaction. However, in spite of preferential bindings of cations with aromatic compounds have been often interpreted in electrostatic terms,[23] the high values of the molecular polarizability (α_{Bz} = 10.32 Å^3, α_{HFBz} = 10.74 Å^3)[24−26] indicates that the non electrostatic contributions, such as induction and dispersion effects, which complicate their quantum chemical treatment, cannot be neglected. Moreover, the different ion size (much larger for negative ions), which modulates the exchange repulsion component, directly affects the features of the aggregates.

All these effects, have been considered by us in the development of a semiempirical potential model, based on the decomposition of the nonelectrostatic component of the interaction energy in pair "effective" contributions between centers of two different partners. Our effort was focused on the choice of potential functions[13,14,19,27−39] defined by a limited number of parameters having a physical meaning, related to basic physical properties of the interacting partners. Most of the parameters so defined become transferable from simple to complex systems. The basic property exploited by us is the "electronic" polarizability of atoms, ions, and molecules. The last one can be partitioned through appropriate decomposition schemes,[24,40−43] thus, providing polarizability components that are conservative (transferable) for chemical bonds of the same type and order and for functional groups of the same type (independently of the molecular complexity).[24,40] Moreover, it is also relevant to remember that the atomic and molecular polarizability is the property useful to scale both attraction and repulsion components of the nonelectrostatic interaction[44−46] and the choice of its different partition schemes (see below) depends on the complexity of the investigated system.

The study of the alkali cation−hexafluorobenzene systems, which form equilibrium on plane bifurcated structures similar to those of the halide-Bz ones, appears to be very interesting to investigate the characteristics of the solvation shells in ionic aggregates. In particular, the comparison of the solvation shells of K^+—HFBz and of Cl^-—Bz is intriguing because of the similar equilibrium energies of the unsolvated aggregates, equal to −392 and −317 meV,[47] respectively. However, some differences in the ion−solvent interaction components can promote pronounced changes in the propensities of the solvation phenomena.

In the present paper, our interest focuses on the Ar microsolvation processes of the K^+—HFBz aggregates, analyzing in detail some similarities and differences in comparison with the characteristics of the Ar-solvated Cl^-—Bz. The study is performed by carrying out MD simulations using the DL_POLY code,[48] from which the Ar three-dimensional (3D) probability around K^+—HFBz is derived. In section 2 the formulation of the potential energy function is outlined, in section 3 the unsolvated K^+—HFBz and Cl^-—Bz systems are compared, and in section 4 the details of MD simulations are given. Results for the K^+-HFBz-Ar and the K^+-HFBz-Ar$_n$ aggregates are presented and analyzed in sections 5 and 6, respectively. In section 7 the evolution from microenvironment arrangement to the solvation processes is discussed. Finally, concluding remarks are given in section 8.

2. ION−BOND AND ION−ATOM INTERACTIONS

The intermolecular interaction between K^+ and HFBz has been described before[47] and here only some details, relevant for this study, are given. Two different decompositions of the HFBz molecular polarizability, depending on the system dimension, have been exploited. In one of them, applied to the study of the smaller K^+-HFBz-Ar$_n$ ($n \leq 15$) aggregates, the molecular polarizability is decomposed in bond components (CC and CF), allowing to describe the K^+—HFBz the Ar—HFBz interactions as combination of ion-bond and atom-bond terms. This approach allows to directly include many body effects due to the formation of chemical bonds. In the other one, the HFBz molecular polarizability has been decomposed in "effective" atomic (C_{eff} and F_{eff}) components (i.e., having different values in respect to the polarizability of the isolated atoms),[42,43] which have been applied to derive the Ar—HFBz interaction as a combination of independent atom-effective atom contributions. This description has only been used when the larger ensembles of Ar atoms are considered (n = 50, 100, 200, and 500).

The total intermolecular interaction, for the Ar-solvated K^+—HFBz, V_{total}, is then formulated as

$$V_{total} = V_{K^+-HFBz} + \sum_{i=1}^{n} V_{Ar_i-HFBz} + \sum_{i=1}^{n} V_{K^+-Ar_i} + \sum_{i=1}^{n-1}\sum_{j>i}^{n} V_{Ar_i-Ar_j} + V_{el} \quad (1)$$

where the electrostatic component V_{el} is defined as the sum of coulomb contributions,[49,50] each one evaluated from the ion charge (K^+ or Cl^-) and from the charge distribution on the HFBz or Bz molecular frame. The remaining terms, whose sum provides the nonelectrostatic component (V_{nel}) of V_{total} are represented as combination of improved Lennard-Jones functions (V_{ILJ}), each one depending, in general, on the distance and the relative orientation of the considered interaction pair. Such model potential, whose reliability and flexibility has been discussed extensively elsewhere,[36,37] basically exploits two scale parameters defining the well depth (ε) and the equilibrium distance (r_0) representative of each interaction pair, whose values can be anticipated by using charge and polarizability components of the involved pair[44−46] (for this reason the parameters can be considered transferable[47]). The ILJ function is represented as[36,51]

$$V_{ILJ} = \varepsilon\left[\frac{m}{\beta + 4.0\left(\frac{r}{r_0}\right)^2 - m}\left(\frac{r_0}{r}\right)^{\beta + 4.0\left(\frac{r}{r_0}\right)^2} - \frac{\beta + 4.0\left(\frac{r}{r_0}\right)^2}{\beta + 4.0\left(\frac{r}{r_0}\right)^2 - m}\left(\frac{r_0}{r}\right)^m\right] \quad (2)$$

where β is the only nondirectly transferable parameter because weakly depending on the environmental conditions,[52] for which

Table 1. Perpendicular and Parallel Components of the Well Depth ($\varepsilon_\perp$, $\varepsilon_\parallel$) and of the Equilibrium Distances ($r_{0\perp}$, $r_{0\parallel}$) for the K^+−CC, K^+−CF, Cl^-−CC, Cl^-−CH, Ar−CC, Ar−CF and Ar−CH Ion/Atom Bond Interactions[a]

ion(atom) bond	$\varepsilon_\perp$ (meV)	$\varepsilon_\parallel$ (meV)	$r_{0\perp}$ (Å)	$r_{0\parallel}$ (Å)	β
K^+−CC	22.95	75.77	3.266	3.547	8.5
K^+−CF	37.75	46.60	3.074	3.365	8.5
Cl^-−CC	16.37	59.64	3.832	4.073	7.0
Cl^-−CH	25.48	28.60	3.655	3.839	7.0
Ar−CC	3.895	4.910	3.879	4.189	9.0
Ar−CF	6.290	5.239	3.674	3.983	9.0
Ar−CH	4.814	3.981	3.641	3.851	9.0

[a] The values of the β parameter are also given.

here we select those values correctly providing the energetic of all dimers obtained via dissociation of the aggregate.[47,51]

The consideration of 12 bond polarizabilities (6 CC and 6 CF) and their further decomposition in perpendicular ($\perp$) and parallel ($\parallel$) components allows to define and to determine the values of the other relevant parameters, ε and r_0, from $\varepsilon_\perp$ and $r_{0,\perp}$, associated to perpendicular approaches of the ion (or atom) to the bond, and $\varepsilon_\parallel$ and $r_{0,\parallel}$, which correspond to approaches of the ion (or the atom) along the bond. These perpendicular and parallel components of ε and r_0 can be anticipated as discussed in ref 36 (see also references therein). This model potential, based on the decomposition of the molecular polarizability, has been widely tested by comparing, for several systems, predictions with accurate ab initio calculations[32,37,52−54] and high level experimental data.[51]

This procedure, used to represent the first (and second) term in eq 1 as a sum of 12 independent ion(atom)−bond interactions is here applied to investigate the small K^+-HFBz-Ar_n aggregates ($n \leq 15$). Accordingly, the first and second terms in eq 1 are decomposed in 6 K^+−CC and 6 K^+−CF and in 6 Ar−CC and 6 Ar−CH interaction contributions. On the contrary, for systems containing more than 15 Ar atoms, the second term in eq 1, after decomposing the molecular polarizability in "effective" C and F polarizabilities, is expressed as a sum of Ar−C_{eff} and Ar−F_{eff} contributions. In this case, the potential parameters do not depend on the approach of the ion (or the atom) to a bond. The K^+−Ar and Ar−Ar interactions are also represented as a combination of ILJ functions.[30,51]

The parameters of the three-body and two-body interactions are given in Tables 1 and 2, respectively. The value of m (in eq 2) has been taken equal to 4 for ion−neutral interactions and equal to 6 for the neutral−neutral ones.

The values of the charges and their positions, used to define V_{el}, are chosen to reproduce the correct components of the HFBz quadrupole moment,[20] and a charge of −0.12 au on each F atom and to two positive charges of 0.06 au, separated by 0.137 Å, for each C atom (above and below the aromatic plane) have been considered.

3. STATIC PROPERTIES OF THE SMALL AGGREGATES

The equilibrium geometry of the Bz−Ar and HFBz−Ar aggregates is very similar, with the Ar atom placed along the C_6 rotational axis of the molecules and at the same distance (R = 3.53 Å) from the center of mass (c.m.) of the aromatic rings. The Bz−Ar and HFBz−Ar energies, at equilibrium, are −45 and −52 meV, respectively. On another hand, due to the similar

Table 2. Well Depth (ε) and Equilibrium Distance (r_0) for the K^+−Ar, Cl^-−Ar, Ar−Ar, Ar−C_{eff}, and Ar−F_{eff} Interaction Pairs (Ar−C_{eff} and Ar−F_{eff} are Used To Describe Ar−HFBz Interactions for n > 15)[a]

ion(atom)−atom	ε (meV)	r_0 (Å)	β
K^+−Ar	110.00	3.190	8.9
Cl^-−Ar	64.87	3.710	7.8
Ar−Ar	12.37	3.757	9.0
Ar−C_{eff}	6.000	3.944	9.0
Ar−F_{eff}	6.152	3.550	9.0

[a] The values of the β parameter are also given.

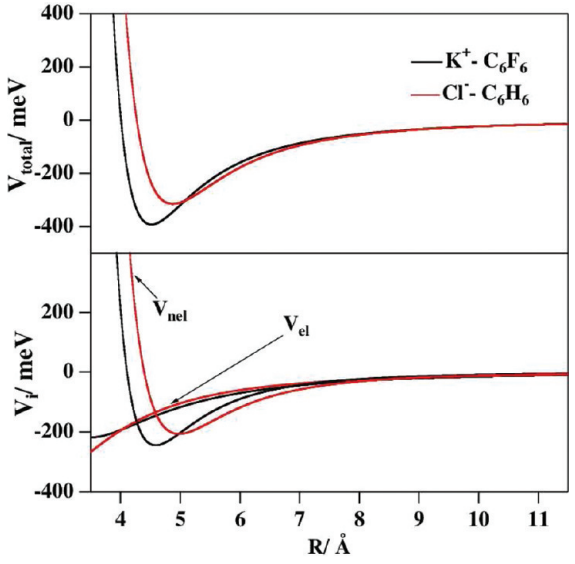

Figure 1. (Top) K^+−HFBz and Cl^-−Bz potential energy curves for on plane approaches of the ions and bisecting the CC bonds. (Bottom) Electrostatic, V_{el}, and nonelectrostatic, V_{nel}, energy contributions for the same approaches. K^+−HFBz (black) and Cl^-−Bz (red).

magnitude and different sign of the quadrupole moment of HFBz and Bz, the K^+−HFBz and Cl^-−Bz interactions assume comparable values. As it has been indicated before, at equilibrium, both K^+−HFBz and Cl^-−Bz show bifurcated on plane structures with the ions placed along an axis bisecting one of the CC bonds of the aromatic rings. For this reason, we have considered approaches on the plane of a given ion, to the c.m. of the aromatic compound bisecting a CC bond, to evaluate the potential energy as a function of the distance R from the ion to the molecule c.m. The corresponding results are given in the top panel of Figure 1. K^+−HFBz, with an equilibrium energy of −392 meV, is stabler than Cl^-−Bz, for which the corresponding energy is of −317 meV. The equilibrium distance of 4.516 Å for K^+−HFBz and 4.875 Å for Cl^-−Bz differs by about 8%. As it can be seen in the figure, the repulsive wall for K^+−HFBz appears at shorter distances than for Cl^-−Bz. This can be explained taking into account the different ion size repulsion, as indicated by the higher polarizability of Cl^- (3.82 $Å^3$) with respect to that of K^+ (0.85 $Å^3$).[44,45] As a matter of fact, as it can be seen in the lower panel of Figure 1, while the electrostatic contribution is very similar for both aggregates, even at distances shorter than the equilibrium ones, the nonelectrostatic one is not, originating differences more pronounced on the equilibrium distances. Nevertheless, the relatively

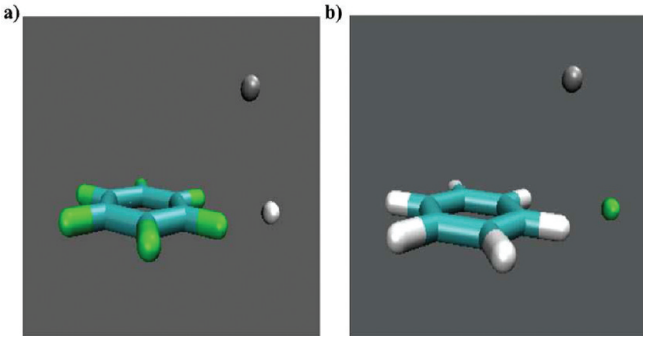

Figure 2. K^+-HFBz-Ar (a) and the Cl^--Bz-Ar (b) equilibrium configurations. The Ar atoms are represented in gray color.

similar geometry of both K^+—HFBz and Cl^-—Bz aggregates may suggest similar solvation shells and as a first step of the study, the binding energy and the equilibrium geometry of the K^+-HFBz-Ar and Cl^--Bz-Ar aggregates have been determined starting from the equilibrium structures of the unsolvated K^+—HFBz and Cl^-—Bz systems. At the equilibrium and with HFBz on the *xy* plane and K^+ in the *x* axis, the Ar atom is placed on the *xz* plane at $x = 3.4415$ Å and $z = 3.0111$ Å.

Results show that while for (K^+-HFBz)-Ar, the binding energy is equal to 533 meV with the Ar atom placed at $R = 4.5$ Å from the center of the aromatic ring, for (Cl^--Bz)-Ar, the binding energy is 407 meV and $R = 4.3$ Å. The K^+-HFBz-Ar and Cl^--Bz-Ar equilibrium configurations are shown in Figure 2a and 2b, respectively. As it can be seen, both equilibrium geometries are very similar, with the Ar atom interacting with both the aromatic compound and the respective ion.

4. SIMULATION DETAILS

Dynamics simulations of the Ar-solvated K^+—HFBz systems have been carried out using the DL_POLY software.[48] The HFBz aromatic compound, as was made for the X^--Bz systems, has been kept rigid in all calculations. A time step of 1 fs has been used in all the simulations presented here, integrating the MD trajectories up to final time of 14 ns. The time step chosen is large enough to keep the fluctuations of E_{total} well below 10^{-5} meV. MD simulations are preceded by an initial equilibration period of 0.1 ns (using the same time step) during which the velocities of all atoms are rescaled to match the input temperature. The equilibration period has been excluded from the statistical analysis at the end of any trajectory. All initial configurations have been generated by placing the K^+—HFBz dimer close to its minimum energy configuration and then solvating it by randomly placing Ar atoms, following the same procedure used before to investigate the Ar-solvated X^-—Bz aggregates.[17,18] The size of the K^+-HFBz-Ar_n smaller clusters investigated here ranges from aggregates containing one single Ar atom to systems containing up to 15 Ar atoms and then MD simulations of the K^+-HFBz-Ar_n (n = 1, ..., 15) have been performed. Moreover, to analyze the aggregate rearrangement to the solvation process, groups of 50, 100, 200, and 500 Ar atoms placed inside a cubic box bearing periodic boundary conditions, have been used. To equilibrate the ensemble of Ar atoms at a given temperature the volume of the cubic box has been selected to reproduce the density of Ar at the chosen temperature T.[19] The trajectories, analyzed under different conditions using a NVE ensemble of particles, have been run over increasing values of the total energy (E_{total}), by starting a new equilibration period from the final configuration, velocities and forces of the previous run. The mean value of both kinetic (and T) and potential energy contributions, E_{kin} and E_{cfg}, respectively, are obtained from the corresponding values monitored over the MD trajectory. This means that E_{cfg} is defined as the average of the total potential energy over all the accessible configurations for a given value of E_{total}. To analyze energy results, E_{cfg} has been further decomposed in three contributions associated with K^+—HFBz (E_{K^+-HFBz}) and Ar—HFBz ($E_{Ar-HFBz}$) and to ion/atom—atom pairs (E_{pairs}), the last including all Ar—Ar and K^+—Ar interactions.

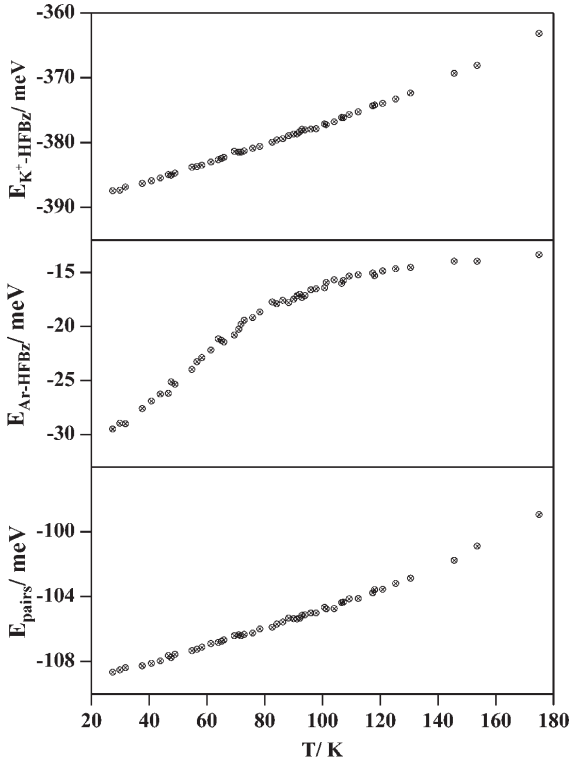

Figure 3. E_{K^+-HFBz} (top panel), $E_{Ar-HFBz}$ (middle panel), and E_{pairs} (lower panel) energy contributions to E_{cfg} for the K^+-HFBz-Ar aggregate.

5. K^+-HFBz-Ar AGGREGATE

The aggregate that HFBz forms with K^+ and only one Ar atom has been investigated at increasing values of E_{total} (and of T). In Figure 3, the dependence of the E_{K^+-HFBz}, $E_{Ar-HFBz}$, and E_{pairs} energy contributions are represented as a function of the temperature in the top, middle, and lower panels, respectively. While both E_{K^+-HFBz} and E_{pairs} vary almost linearly with T, $E_{Ar-HFBz}$ shows a sigmoidal shape due to a higher increase of $E_{Ar-HFBz}$ (less negative values of the energy) at low temperatures in respect of that observed at higher T: while an increases of about a 40% is observed in the 30—80 K temperature range, $E_{Ar-HFBz}$ increase less than 30% when the temperature goes from 80 to 170 K. Such sigmoidal shape is very similar to that of E_{Ar-Bz}, previously obtained for the Cl^--Bz-Ar aggregate.[17] However, at a given temperature, Cl^--Bz-Ar dissociates more likely in Cl^--Bz+Ar than K^+-HFBz-Ar in K^+-HFBz+Ar. As a matter of fact, Cl^--Bz-Ar and K^+-HFBz-Ar promote such dissociation with a high probability at temperatures of about 100 and 160 K, respectively.

Table 3. Number of Ar Atoms, n, Configuration Energy, E_{cfg}, and the E_{K^+-HFBz}, $E_{Ar-HFBz}$, and E_{pairs} Energy Contributions in the K^+-HFBz-Ar_n Aggregates at a Temperature of about 30 K

n	E_{cfg} (meV)	E_{K^+-HFBz} (meV)	$E_{Ar-HFBz}$ (meV)	E_{pairs} (meV)
2	−651	−385	−45	−221
3	−800	−387	−68	−345
4	−938	−387	−78	−473
5	−1066	−385	−78	−603
6	−1234	−387	−92	−754
7	−1396	−387	−103	−906
8	−1532	−386	−107	−1039
9	−1615	−386	−149	−1080
10	−1749	−386	−138	−1225
11	−1815	−385	−175	−1255
12	−1910	−385	−218	−1307
13	−1983	−384	−246	−1353
14	−2009	−383	−240	−1386
15	−2064	−382	−266	−1416

An analysis of the different energy contributions reveals that, at a given temperature, the $E_{Ar-HFBz}$ and E_{Ar-Bz} energy contributions are very similar, even when the dissociation probability is high. Accordingly, the higher stability of K^+-HFBz-Ar in comparison with Cl^--Bz-Ar is mainly due to the interaction between Ar and the corresponding ion. As it can be observed in the middle panel of Figure 3, the energy results for the K^+-HFBz-Ar aggregate indicate that, by increasing T, $E_{Ar-HFBz}$ tends to an energy plateau of −13 meV, as it has been observed for the E_{Ar-Bz} contribution associated to the Cl^--Bz-Ar aggregate. On the contrary, E_{pairs} depends on the aggregate. For instance, at the higher temperature investigated, E_{pairs} is equal to −103 meV for K^+-HFBz-Ar, which differs only about a 6% in respect of the K^+-Ar equilibrium energy (−110 meV), while E_{pairs} amounts to −53 meV for Cl^--Bz-Ar, which differs of about a 20% in respect of the Cl^-−Ar equilibrium energy (−65 meV).

6. K^+-HFBz-Ar_n AGGREGATES

To assess the energetics and to understand the main features of the Ar-solvated K^+−HFBz dimer, the K^+-HFBz-Ar_n ($n \leq 15$) aggregates have been investigated by performing MD simulations, at similar values of the mean temperature, in which the number of Ar atoms has been increased systematically. The energy contributions defined in the previous section have been analyzed as a function of T and it has been observed that, for a given temperature (or total energy), maintained below the cluster dissociation limits, the E_{K^+-HFBz} energy contribution remains essentially constant, that is, independent of n, indicating that the presence of a large or small number of Ar atoms in the cluster does not disrupt the preferred geometry of the K^+−HFBz aggregate. The values of the other energy contributions (E_{K^+-HFBz}, $E_{Ar-HFBz}$, and E_{pairs}), at a temperature of about 30 K, are given in Table 3. Bearing in mind that E_{K^+-HFBz} does not change by increasing n, the observed E_{cfg} decrease (more negative values) must be due to the increase of n, which originates stronger contributions of both $E_{Ar-HFBz}$ and E_{pairs} (E_{pairs} dominating on $E_{Ar-HFBz}$). The decrease of $E_{Ar-HFBz}$ by increasing n does not follow a clear linear tendency, as it was also observed for the E_{Ar-Bz} energy contribution associated to the X^-−Bz

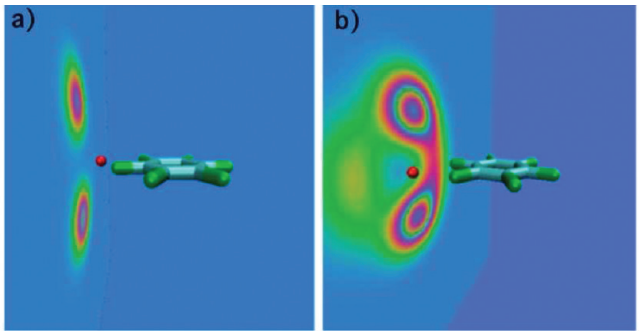

Figure 4. Two-dimensional maps of the probability density of Ar atoms around the K^+−HFBz aggregate: the case of 2 and 3 Ar atoms is reported in (a) and (b), respectively, at a temperature of 30 K.

aggregates.[17,18] This behavior can be related to the compactness of the solvation shell, which depends on the number of Ar atoms.

The changes in the solvation shell, due to an increase of the number of Ar atoms, have been also studied by considering the three-dimensional (3D) probability density, evaluated by introducing our simulation data (properly shifted to the inertial reference frame) into the VMD visualization program. The Volmap tool[55] included in the mentioned package allowed us to visualize two-dimensional (2D) slices from a volumetric data set and isosurfaces of (mass weighted) constant probability density for the Ar atoms. These isosurfaces can be interpreted as "argon orbitals" (see, for instance, refs 17 and 18). In Figure 4, where a 2D representation of the volumetric probability density for K^+-HFBz-Ar_2 (left panel) and K^+-HFBz-Ar_3 (right panel) are represented, it can be seen that the Ar atoms prefer to be placed above and below the HFBz plane and close to K^+ on an axis parallel to the C_6 rotational axis of HFBz. When n increases, as it was observed for the solvation of Cl^--Bz,[17,18] the Ar atoms tend to be placed around the cation. However, the higher stability of both K^+−HFBz and K^+−Ar in comparison with that of Cl^-−Bz and Cl^-−Ar, originates some differences on the respective solvation spheres. These differences can be understood considering that (1) in the K^+−HFBz dimer, at equilibrium, K^+ is placed closer to the center of mass of the aromatic ring than Cl^- in Cl^-−Bz, (2) the Cl^-−Ar equilibrium distance is larger than the K^+−Ar one, and (3) the Ar−Bz equilibrium distance almost coincides with the corresponding one on Ar−HFBz. Therefore, the Ar atoms tend to occupy approximately the same position when interacting with either Bz or HFBz. However, as K^+ is closer to the center of aromatic ring, some positions of Ar atoms behind the ion in K^+−HFBz are stabilized by both Ar−K^+ and Ar−HFBz interactions, while in the case of Cl^-−Bz, those Ar atoms placed behind chlorine, due to the larger distance, interact less effectively with Bz. As it can be seen in Figure 5, where two different perspectives of a three-dimensional probability density of the Ar atoms in the K^+-HFBz-Ar_6 aggregate are shown, unlike the results obtained for the Ar-solvated Cl^-−Bz,[17] 6 Ar atoms do not tend to form a unique circle around K^+−HFBz. For Cl^--Bz-Ar_6, the 3D probability density plots seemed to indicate practically a free rotation of all Ar atoms around Cl^-−Bz,[17,18] while for K^+-HFBz-Ar_6, it seems that only 4 Ar atoms rotate freely around K^+−HFBz. The experimental evidence of an almost-free internal rotation on adducts containing aromatic compounds has been reported in the literature.[56] Moreover, due to the favored positions behind K^+, allowing the Ar atoms to interact with both

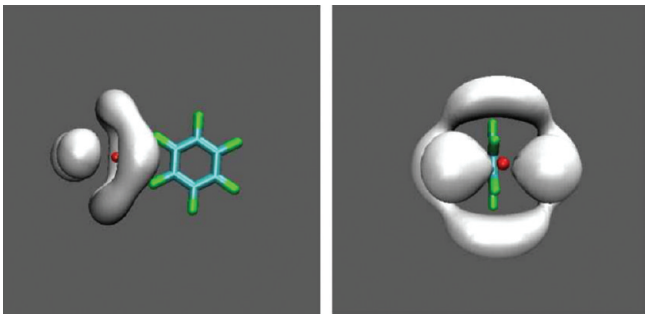

Figure 5. Different views of isosurface (0.8) plots of the Ar probability density in the K^+-HFBz-Ar_6 aggregates at a temperature of 30 K.

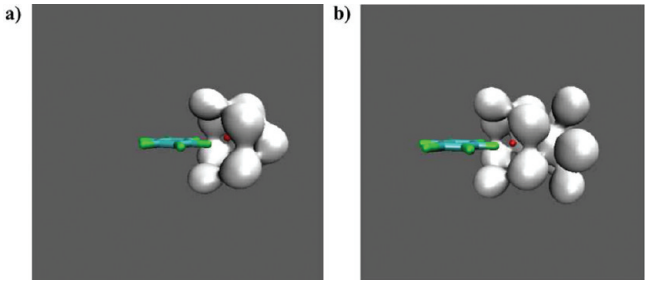

Figure 6. Isosurface (isovalue: 0.8) plots of the Ar probability density: K^+-HFBz-Ar_{10} (a) and K^+-HFBz-Ar_{15} (b) at a temperature of 30 K.

K^+ and HFBz, the cation is more efficiently solvated than the anion. This fact contrasts with the characteristics of the solvation when cation and anion are simultaneously present. For instance, the Ar-solvated Na^+-Bz-Cl^- aggregates show the Ar atoms placed preferably close to Cl^-.[19] However, it must be pointed out that in the equilibrium configuration of Na^+-Bz-Cl^-, Na^+ is placed along the rotational axis of Bz and Cl^- lies close to Na^+.

By further increasing n it has been observed that the most compact solvation shells are obtained with 10 and 15 Ar atoms, which tend to form symmetric compacted structures around K^+—HFBz, as it can be seen in Figure 6. In the less compact structures of the K^+-HFBz-Ar_n aggregates (n = 3, 5, 7, 8, 9, 11, 12, 13 and 14) some of Ar atoms can occupy several places around K^+—HFBz, forming different structures having similar energies (less compacted shells). This is shown in Figure 7 for K^+-HFBz-Ar_{11}, where the additional atom (respect to n = 10) tends to move away. The different characteristics of the solvation shells for the K^+-HFBz-Ar_{10} and K^+-HFBz-Ar_{11} aggregates are reflected in the radial distribution functions (RDF), as it can be appreciated in Figure 8, where the RDF of the Ar atoms respect the c.m. of HFBz are shown. As it can be seen, the less structured RDF is for the more "rigid" K^+-HFBz-Ar_{10} structure. The RDF for K^+-HFBz-Ar_9, with an incomplete "rigid" solvation shell, is more structured than that for K^+-HFBz-Ar_{11}, for which 10 of the Ar atoms form a compact structure and only the additional Ar is free to move around K^+—HFBz. Moreover, the aggregates forming less compact structures isomerize in a easier way than those forming more compact groups of atoms. This can be seen in Figure 9 where the values of the distance from two Ar atoms of K^+-HFBz-Ar_{14} to the HFBz c.m. show noticeable fluctuations along the trajectory. In the low panel, for K^+-HFBz-Ar_{15}, no changes on the distances (except those corresponding to vibrations) from Ar atoms to HFBz are observed. This behavior

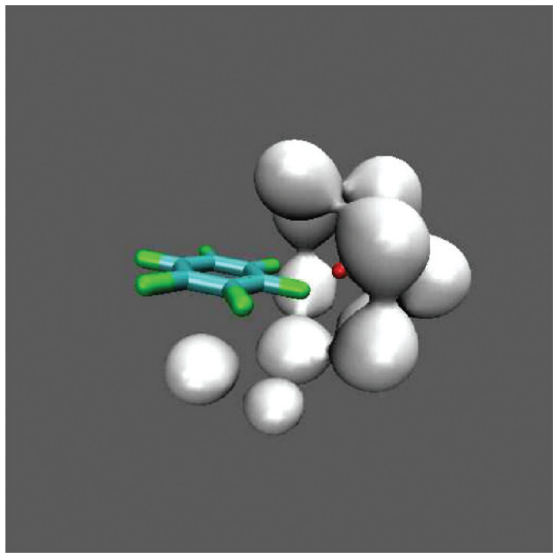

Figure 7. Isosurface (isovalue: 0.8) plot of the Ar probability density for K^+-HFBz-Ar_{11} at a temperature of 30 K.

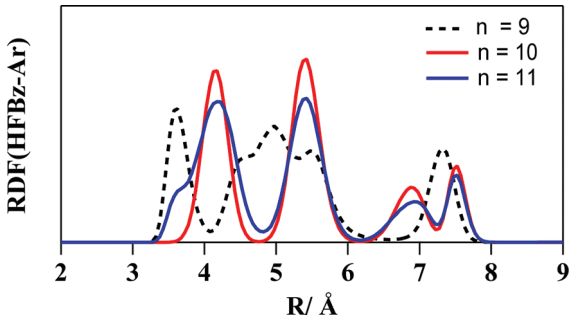

Figure 8. Radial distribution functions, RDF, of three K^+-HFBz-Ar_n aggregates. R is the distance from Ar atoms to the center of mass of HFBz. Results are provided by MD simulations at a temperature of 30 K.

is independent of the selected Ar atom. On the contrary, in the top panel of the figure, noticeable variations on the distance values, indicating an isomerization process, are observed for the K^+-HFBz-Ar_{14} aggregate, which, as it has been indicated, exhibits a structure less compacted than K^+-HFBz-Ar_{15}.

7. FROM CLUSTER REARRANGEMENT TO SOLVATION DYNAMICS

In order to analyze the evolution from the cluster rearrangement discussed above to the solvation dynamics, ensembles of 50, 100, 200, and 500 Ar atoms have been taken into account. The characteristics of the Ar as a solvent has been analyzed in a previous paper considering an ensemble of 500 atoms.[19] Specifically such ensemble was used to investigate the solvation of Bz and of the Bz-Cl^--Na^+ aggregate.[19] Moreover, as stressed above, the simultaneous presence in the cluster of many Ar atoms requires a simplified representation of the full interaction given in terms of a combination of Ar—atom "effective" pairs. This procedure has been also adopted in the present study and the first step has been to compare, for the HFBz—Ar dimer, the predicted results of atom—atom and atom—bond approaches concerning both the energy and the geometry at equilibrium.

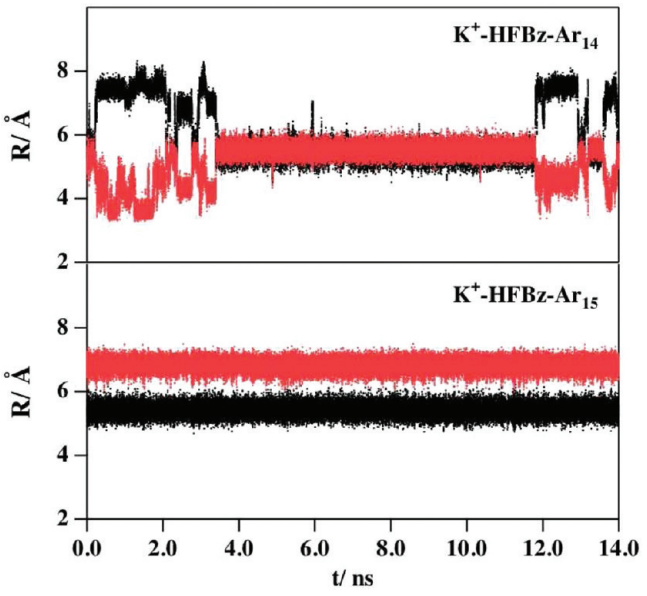

Figure 9. (Top) Evolution along the trajectory of the distance from two selected Ar atoms to the center of mass of HFBz for the K^+-HFBz-Ar_{14} aggregate at 30 K; (Bottom) as above for K^+-HFBz-Ar_{15} aggregate.

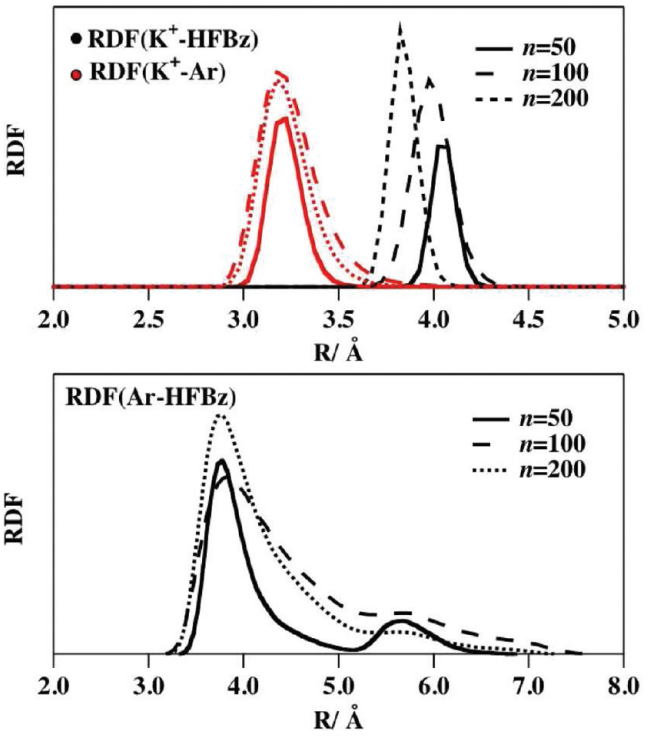

Figure 10. Radial distribution functions, RDF, for K^+—HFBz and K^+—Ar (top) and Ar—HFBz (bottom). In the RDFs for K^+—HFBz and Ar—HFBz, *R* is the distance from K^+ and Ar to the c.m. of HFBz, repectively, while for the K^+—Ar RDF, *R* is the distance from K^+ to Ar. Results are provided by MD simulations at a temperature of 100 K.

Results show only small differences of about 2 and 1% on the potential energy and distances at equilibrium, respectively. However, it must be stressed again that the atom—atom decomposition has been realized and tuned up (see also ref.[19]) by comparing results obtained on the more simplest aggregates from the atom—atom and the (most accurate) atom—bond partitions,[47] and by using effective polarizability values consistent with data from the literature.[42,43]

The effect of going from n = 50 to n = 500 has been first analyzed by considering K^+—HFBz, Ar—HFBz (referred to the HFBz c.m.), and K^+—Ar radial distribution functions. Results show that, the K^+—Ar RDF peaks at the same distance between cation and Ar atoms, independently of n. On the contrary, by increasing n, the K^+—HFBz RDF peaks at shorter cation-molecule distances. The corresponding RDFs are shown in the top panel of Figure 10, where the results for n = 500 have not been included due to the difference in the peak heights in comparison with results for other n values. The position of the K^+—HFBz RDF peak, appearing at shorter distances as the number of Ar atoms increases, could indicate that K^+ tends to occupy positions out of the aromatic plane, so that more repulsive zones of the K^+—HFBz dimer potential energy surface are involved. As it can be seen in Table 4 the E_{K^+-HFBz} contribution assumes less negative values with the increase of the Ar atom number. This result contrasts with that obtained for the small aggregates ($n \leq 15$) given in Table 3 and clearly indicates that the dissociation probability of the K^+—HFBz dimer here increases considerably due to the solvation process. On the lower panel of Figure 10 the Ar—HFBz RDFs are represented, where it can be observed the tendency to form an unique solvation shell as n increases. To further analyze the disposition of the Ar atoms around K^+—HFBz, the 3D representations of the Ar probability density have ben also analyzed. The 3D representations show that for n = 50, two groups of the Ar atoms tend to occupy positions close to the rotational axis of HFBz, above and below of the aromatic plane. A third group, at the beginning

Table 4. Number of Ar Atoms, *n*, and E_{K^+-HFBz} at a Temperature of about 100 K

n	50	100	200	500
E_{K^+-HFBz} (meV)	−180	−152	−109	−71

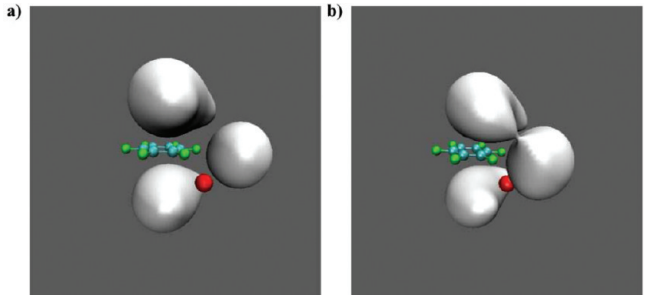

Figure 11. Isosurfaces (isovalue: 0.8) plots of the Ar probability density for K^+-HFBz-Ar_{50} at a temperature of 50 (a) and 100 K (b).

of the trajectory, placed behind the cation, along the trajectory pushes K^+ bringing it close to another group of atoms. The solvated ion, moves from the equilibrium position on the dimer as it can be observed in Figure 11. This configuration is quite stable because no noticeable changes on the structure are observed when the temperature is increased. However, by increasing T, the K^+ solvation takes place in a more extent as it can be seen in Figure 11. By further increasing the number of Ar atoms it can be observed, in agreement with Ar—HFBz RDFs,

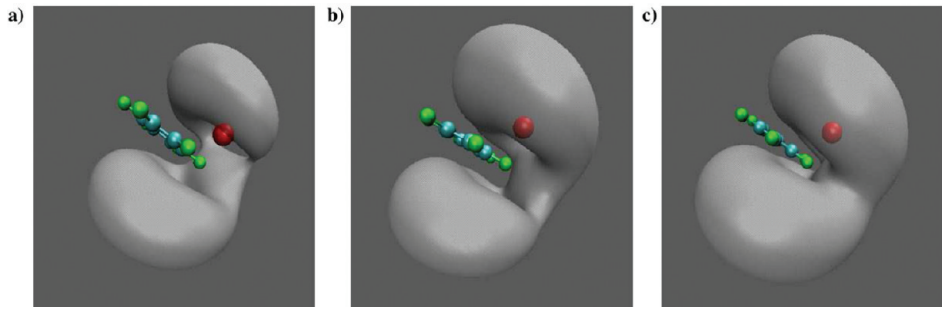

Figure 12. Isosurfaces (isovalue: 3.0) plots of the Ar probability density around K^+—HFBz at a temperature of 100 K. Number of Ar atoms: 100 (a), 200 (b), and 500 (c).

the tendency of Ar atoms to form a single solvation shell around K^+—HFBz (see Figure 12). Such figure also shows that the extent of the cation solvation increases with the number of Ar atoms. In general, the solvation of the cation contrasts with that of the aromatic compound and the solvation shells, in all cases, are asymmetric and the Ar atoms are placed close the cation, while the opposite side of the molecule remain unsolvated, even when 500 Ar atoms are considered.

8. CONCLUDING REMARKS

Solvation effects on K^+—HFBz have been investigated by employing Ar atoms as a solvent species, which have been randomly distributed around the ionic dimer. Ar atoms are popular surrogates of water molecules, mainly because of their similar polarizability. The transition between the K^+-HFBz-Ar_n cluster rearrangement and solvation dynamics has been investigated by performing MD simulations under different initial conditions. An analytical potential energy function constructed as combination of two-body, three-body (atom(ion)—bond) contributions has been employed for this purpose, representing both the two-body and the three-body nonelectrostatic components by means of the ILJ function. The electrostatic contribution has been calculated using the Coulomb law, which has been applied between the charge of ions and punctual charges placed on the aromatic molecules. This formulation of the interaction preserve the asymptotic behavior of the ion—quadrupole interaction. The cluster rearrangement has been investigated by systematically adding Ar atoms ($n \leq 15$) to K^+—HFBz. It has been observed that "magic" numbers of Ar atoms, as for instance $n = 4, 6, 10$, and 15, provide compact structures around the dimer. It has been also observed that the isomerization process for K^+—HFBz, when solvated by "magic" numbers of Ar atoms forming very stable and compact aggregates, is less probable that for less compacted structures. The microenvironments associated with different minima in the potential energy surface have been investigated by performing a 3D analysis of the Ar atoms probability density, derived from our MD simulations. The different role played by the leading interaction components in aggregates formed by Bz and HFBz molecules and atomic ions has been evidenced by comparing the Cl^-—Bz and the K^+—HFBz aggregates, which have similar energy and geometry at equilibrium. In spite of these similarities, the small changes in the interacting features of the involved atom/ion—atom/molecule pairs influence the disposition of the Ar atoms around the dimers, originating differences in the incomplete solvation shells. As a matter of fact, the small differences on the equilibrium distances from the ions to the respective aromatic compound and the pronounced variation of the K^+—Ar and Cl^-—Ar interaction pairs cause significant variations in the features of microsolvation environments. Bearing in mind that K^+ and Cl^- are isoelectronic, it seems that the differences can be attributed to the different size of ions. The solvation process has been investigated considering ensembles of 50, 100, 200, and 500 Ar atoms from which MD calculations have ben performed. Results indicate that the Ar atoms tend to push apart K^+ from the equilibrium position on the K^+—HFBz dimer, reaching more repulsive zones of its potential energy surface. Accordingly, the dissociation probability increases considerably with the number of Ar atoms, indicating that the dissociation process is favored by solvation. The preference of Ar atoms to solvate K^+ better than HFBz has been observed.

AUTHOR INFORMATION

Corresponding Author
*E-mail: m.alberti@ub.edu.

ACKNOWLEDGMENT

M.A. acknowledges financial support from the Ministerio de Educación y Ciencia (Spain, Projects CTQ2010-16709 and PR2010-0243) and the Generalitat de Catalunya (Project 2009-SGR 17). Also, thanks are due to the Centre de Supercomputació de Catalunya CESCA-C4 and Fundació Catalana per a la Recerca for the allocated supercomputing time. F.P. and N.F.L. acknowledge financial support from the Italian Ministry of University and Research (MIUR) fo PRIN Contracts. N.F.L. also acknowledges the European Community's Seventh Framework Programme (FP7/2007-2013) because one part of research leading to these results has received funding under Grant Agreement No. 242311 and thanks also are due for financial support to INSTM.

REFERENCES

(1) Sogas, J.; Aricha, M. E.; de Andrés, J.; Albertí, M.; Lucas, J. M.; Aguilar, *A. Phys. Chem. Chem. Phys.* **2001**, *3*, 3638.
(2) Casavecchia, P.; Capozza, G.; Segoloni, E.; Leonori, F.; Balucani, N.; Volpi, G. G. *J. Phys. Chem. A* **2005**, *109*, 3527.
(3) Albertí, M.; Pietro, M.; Aguilar, A. *J. Chem. Soc., Faraday Trans.* **1992**, *88*, 1615.
(4) Albertí, M.; Sayós, R.; Solé, A.; Aguilar, A. *J. Chem. Soc., Faraday Trans.* **1991**, *87*, 1057.
(5) Bargueño, P.; Jambrina, P. G.; Alvariño, J. M.; Hernández, M. L.; Aoiz, F. J.; Menéndez, M.; Verdasco, E.; González-Lezana, T. *J. Phys. Chem. A* **2009**, *113*, 14237.

(6) Martínez, T.; Hernández, M. L.; Alvariño, J. M.; Laganà, A.; Aoiz, F. J.; Menéndez, M.; Verdasco, E. *Phys. Chem. Chem. Phys.* **2000**, *2*, 589.
(7) Faginas Lago, N.; Costantini, A.; Huarte-Larrañaga, F. *Int. J. Quantum Chem.* **2010**, *110*, 422.
(8) Douin, S.; Parneix, P.; Amar, F. G.; Bréchignac, Ph. *J. Phys. Chem. A* **1997**, *101*, 122.
(9) Dopfer, O.; Nizkorodov, S. A.; Meuwly, M.; Bieske, E. J.; Maier, J. P. *Int. J. Mass Spectrom.* **1997**, *167/168*, 637.
(10) Nakanaga, T.; Ito, F. *Chem. Phys. Lett.* **2002**, *355*, 109.
(11) Solcà, N.; Dopfer, O. *Phys. Chem. Chem. Phys.* **2004**, *6*, 2732.
(12) Dopfer, O. *J. Phys. Chem. A* **2000**, *104*, 11693.
(13) Albertí, M.; Aguilar, A.; Lucas, J. M.; Laganà, A.; Pirani, F. *J. Phys. Chem. A* **2007**, *111*, 1780.
(14) Huarte-Larrañaga, F.; Aguilar, A.; Lucas, J. M.; Albertí, M. *J. Phys. Chem. A* **2007**, *111*, 8072.
(15) Albertí, M.; Castro, A.; Laganà, A.; Moix., M; Pirani, F.; Cappelletti, D. *Eur. Phys. J. D* **2006**, *38*, 185.
(16) Albertí, M.; Aguilar, A.; Lucas, J. M.; Pirani, F. *Theor. Chem. Acc.* **2009**, *123*, 21.
(17) Huarte-Larrañaga, F.; Aguilar, A.; Lucas, J. M.; Albertí, M. *Theor. Chem. Acc.* **2011**, *128*, 757.
(18) Albertí, M.; Huarte-Larrañaga, F.; Aguilar, A.; Lucas, J. M.; Pirani, F. *Phys. Chem. Chem. Phys.* **2011**, *13*, 8251.
(19) Albertí, M.; Pirani, F. *J. Phys. Chem. A* **2011**, *115*, 6394.
(20) Garau, C.; Frontera, A.; Quiñonero, D.; Ballester, P.; Costa, A.; Deyà, P. M. *J. Phys. Chem. A* **2004**, *108*, 9423.
(21) Luhmer, M.; Bartik, K.; Dejaegere, A.; Bovy, P.; Reisse, J. *Bull. Soc. Chim. Fr.* **1994**, *131*, 603.
(22) Williams, J. H. *Acc. Chem. Res.* **1993**, *26*, 593.
(23) Ma, J. C.; Dougherty, D. A. *Chem. Rev.* **1997**, *97*, 1303.
(24) Hirshfelder, J. O.; Curtiss, C. F.; Bird, R. B. *Molecular Theory of Gases and Liquids*; Wiley: New York, 1964.
(25) Battaglia, M. R.; Buckingham, A. D.; Williams, J. H. *Chem. Phys. Lett.* **1981**, *78*, 421.
(26) Adamo, C.; Cossi, M.; Scalmani, G.; Barone, V. *Chem. Phys. Lett.* **1999**, *307*, 265.
(27) Albertí, M.; Aguilar, A.; Bartolomei, M.; Cappelletti, D.; Laganà, A.; Lucas, J. M.; Pirani, F. *Lect. Notes Comput. Sci.* **2008**, *5072*, 1026.
(28) Albertí, M.; Aguilar, A.; Cappelletti, D.; Laganà, A.; Pirani, F. *Int. J. Mass Spectrom.* **2009**, *280*, 50.
(29) Albertí, M.; Aguilar, A.; Bartolomei, M.; Cappelletti, D.; Laganà, A.; Lucas, J. M.; Pirani, F. *Phys. Script.* **2008**, *78*, 058108.
(30) Faginas Lago, N.; Huarte Larrañaga, F.; Albertí, M. *Eur. Phys. J. D* **2009**, *55*, 75.
(31) Paolantoni, M.; Faginas Lago, N.; Albertí, M.; Laganà, A. *J. Phys. Chem. A* **2009**, *113*, 15100.
(32) Albertí, M.; Faginas Lago, N.; Laganà, A.; Pirani, F. *Phys. Chem. Chem. Phys.* **2011**, *13*, 8422.
(33) Costantini, A.; Albertí, M.; Pirani, F. *Int. J. Quantum Chem.* **2011**, DOI: 10.1002/qua.23060.
(34) Albertí, M.; Castro, A.; Laganà, A.; Pirani, F.; Porrini, M.; Cappelletti, D. *Chem. Phys. Lett.* **2004**, *392*, 514.
(35) Albertí, M. *J. Phys. Chem. A* **2010**, *114*, 2266.
(36) Albertí, M.; Castro, A.; Laganà, A.; Moix, M.; Pirani, F.; Cappelletti, D.; Liuti, G. *J. Phys. Chem. A* **2005**, *109*, 2906.
(37) Albertí, M.; Aguilar, A.; Lucas, J. M.; Pirani, F.; Cappelletti, D.; Coletti, C.; Re, N. *J. Phys. Chem. A* **2006**, *110*, 9002.
(38) Albertí, M.; Aguilar, A.; Lucas, J. M.; Cappelletti, D.; Laganà, A.; Pirani, F. *Chem. Phys.* **2006**, *328*, 221.
(39) Albertí, M.; Pacifici, L.; Laganà, A.; Aguilar, A. *Chem. Phys.* **2006**, *327*, 105.
(40) Denbigh, K. G. *Trans. Faraday Soc.* **1940**, *36*, 936.
(41) Smith, R. P.; Mortensen, E. M. *J. Chem. Phys.* **1960**, *32*, 502.
(42) Ewig, C. S.; Waldman, M.; Maple, J. R. *J. Phys. Chem. A* **2002**, *106*, 326.
(43) Gavezzotti, A. *J. Phys. Chem. B* **2003**, *107*, 2344.
(44) Cambi, R.; Cappelletti, D.; Liuti, G.; Pirani, F. *J. Chem. Phys.* **1991**, *95*, 1852.
(45) Cappelletti, D.; Liuti, G.; Pirani, F. *Chem. Phys. Lett.* **1991**, *183*, 297.
(46) Pirani, F.; Cappelletti, D.; Liuti, G. *Chem. Phys. Lett.* **2001**, *350*, 286.
(47) Albertí, M.; Aguilar, A.; Lucas, J. M.; Pirani, F. *J. Phys. Chem. A* **2010**, *114*, 11964.
(48) http://www.cse.scitech.ac.uk/ccg/software/DL − POLY/.
(49) Maitland, G. C.; Rigby, M.; Smith, E. B.; Wakeham, W. A. *Intermolecular Forces*; Oxford University Press: New York, 1987.
(50) Sunner, J.; Nishizawa, K.; Kebarle, P. *J. Phys. Chem.* **1981**, *85*, 1814.
(51) Pirani, P.; Brizi, S.; Roncaratti, L. F.; Casavecchia, P.; Cappelletti, D.; Vecchiocattivi, F. *Phys. Chem. Chem. Phys.* **2008**, *10*, 5489.
(52) Albertí, M.; Faginas Lago, N.; Pirani, F. *Chem. Phys.* **2011**. DOI: 10.1016/j.chemphys.2011.
(53) Albertí, M.; Aguilar, A.; Lucas, J. M.; Pirani, F.; Coletti, C.; Re, N. *J. Phys. Chem. A* **2009**, *113*, 14606.
(54) Albertí, M.; Aguilar, A.; Pirani, F. *J. Phys. Chem. A* **2009**, *113*, 14741.
(55) Humphrey, W.; Dalke, A.; Schulten, K. *J. Mol. Graphics* **1996**, *14*, 33.
(56) López, J. C.; Caminati, W.; Alonso, J. L. *Angew. Chem., Int. Ed.* **2006**, *45*, 290.